

Article

Lanthanum-Modified Phosphogypsum Red Mud Composite for the Co-Adsorption of Cadmium and Arsenic: Mechanism Study and Soil Remediation

Chengmei Shang^{1,2}, Zhixi Geng³, Yuanyuan Sun^{1,2,*}, Dongxue Che¹, Qingjiao Zhao¹, Ting Chen^{1,2}, Ming Tang^{1,2}  and Lijuan Huo^{4,*}

¹ School of Life Sciences, Guizhou Normal University, Guiyang 550001, China; shchm118@163.com (C.S.); c15185281694@163.com (D.C.); m18286684760@163.com (Q.Z.); 17885811246@163.com (T.C.); mingtang@gznu.edu.cn (M.T.)

² Key Laboratory of National Forestry and Grassland Administration on Biodiversity Conservation in Karst Mountainous Areas of Southwestern China, Guizhou Normal University, Guiyang 550001, China

³ Beijing Zhongnong Jiayuan Eco-Engineering Technology Co., Ltd., Beijing 100043, China; gengzhixi1219@126.com

⁴ School of Environment and Resources, Taiyuan University of Science and Technology, Taiyuan 030024, China

* Correspondence: sunyuanyuan@gznu.edu.cn (Y.S.); hlj@tyust.edu.cn (L.H.)

Abstract: With the development of industrial activities and the agricultural and mining industries, farmland soils are facing serious problems related to heavy metal contamination, especially cadmium (Cd) and arsenic (As) contamination. In this study, two industrial by-products, phosphogypsum (PG) and red mud (RM), were modified by lanthanum (La) impregnation to form a new composite (L-PR) to investigate the adsorption performance of Cd(II)/As(V) in both single and binary systems. The adsorption mechanisms of Cd(II)/As(V) on L-PR were analyzed using SEM, XRD, FTIR, and XPS. The passivation effect of L-PR on the Cd-As composite contaminated soil was confirmed through a soil cultivation experiment. The adsorption experiments revealed that L-PR showed superior adsorption capabilities for Cd(II) and As(V) compared to PG and RM. Additionally, L-PR was found to be less affected by changes in pH. The kinetic studies indicated that Cd(II) and As(V) adsorption by L-PR followed the second-order kinetic model most accurately. Isothermal adsorption experiments revealed that the adsorption of Cd(II) by L-PR was more in accordance with the Freundlich model, while As(V) was more in accordance with the Langmuir model. The mechanisms of Cd(II) and As(V) adsorption on L-PR involved electrostatic attraction, ion exchange, complexation, and precipitation. The adsorption of Cd(II) is dominated by complexation and precipitation, and the adsorption of As(V) is dominated by ion exchange and complexation. Soil cultivation experiments showed that L-PR significantly reduced the available Cd and As concentrations in soil by 86.01% and 27.80%, respectively, and it could induce the transformation of non-stable Cd(II)/As(V) to the more stable residual. In summary, L-PR exhibits facile preparation, excellent adsorption performance, and is capable of simultaneously removing Cd(II) and As(V) from aqueous solutions while immobilizing these contaminants in soil. These remarkable attributes made it a highly promising alternative for the simultaneous treatment of various toxic metal contaminants.

Keywords: industrial by-products; lanthanum; cadmium; arsenic; adsorption



Citation: Shang, C.; Geng, Z.; Sun, Y.; Che, D.; Zhao, Q.; Chen, T.; Tang, M.; Huo, L. Lanthanum-Modified Phosphogypsum Red Mud Composite for the Co-Adsorption of Cadmium and Arsenic: Mechanism Study and Soil Remediation. *Agriculture* **2024**, *14*, 464. <https://doi.org/10.3390/agriculture14030464>

Academic Editor: Ryusuke Hatano

Received: 25 January 2024

Revised: 10 March 2024

Accepted: 11 March 2024

Published: 13 March 2024



Copyright: © 2024 by the authors. Licensee MDPI, Basel, Switzerland. This article is an open access article distributed under the terms and conditions of the Creative Commons Attribution (CC BY) license (<https://creativecommons.org/licenses/by/4.0/>).

1. Introduction

The highly toxic elements cadmium (Cd) and arsenic (As) are classified as class I carcinogens by the International Agency for Research on Cancer (IARC) [1]. When contaminants in aquatic and soil environments exceed regulatory standards and remain unremediated, they pose significant health risks [2,3]. Long-term exposure to Cd and As in humans can result in various diseases. For instance, prolonged exposure to Cd has

been associated with lung cancer, osteoporosis, and spinal deformities [4,5], while the excessive intake of As can lead to skin cancer, liver cancer, bronchitis, acute gastroenteritis, kidney damage, and cardiovascular diseases [5,6]. They are released into aquatic and terrestrial environments mainly through anthropogenic activities such as the discharge of wastewater and sewage, the use of pesticides and fertilizers, the mining of ores, and the burning of fuels, and they accumulate in living organisms through the food chain; they present a significant threat to the environment and human well-being [7–9]. The Report on the National General Survey of Soil Contamination reveals that the farmland soil exceedance rate in China reached a staggering 19.4%, with specific exceedance rates for Cd and As standing at 7% and 2.7%, respectively [10]. Chen et al. showed that approximately 1.4 million hectares of farmland soils in China have been contaminated by irrigation with sewage, 64.8% of which are contaminated with heavy metals [11]. Zeng et al. found that the Cd and As contamination in the soil of vegetable fields in China was severe; sample analysis showed that the exceedance rate of Cd was 24.1%, the exceedance rate of As was 9.2%, and 44.2% of samples exhibited As accumulation [12]. Cd and As are highly toxic, widely distributed contaminants and tend to form complexes, resulting in contamination that is difficult to remediate due to their conflicting chemical properties, which poses a major risk to the quality of agricultural products and ecological safety [13,14]. For Cd-As composite contamination, it is difficult for a single passivation material to achieve good remediation results, and the simultaneous chemical passivation of Cd and As has become an emerging hotspot for heavy metal research.

Scientists are interested in developing passivation materials that are efficient, low-cost, and environmentally beneficial to control the contamination of Cd and As. Phosphogypsum (PG) is a by-product of wet-process phosphoric acid production. It consists mostly of calcium sulfate dihydrate and is known for its acidity, high production volume, and complicated composition. Around 4 to 6 tons of PG is emitted for every ton of phosphoric acid that is manufactured [15,16]. Red mud (RM) refers to the iron oxide-rich by-product generated during the industrial refining of alumina from bauxite ore, which gives it its characteristic red color; the distinguishing features of it include a high level of alkalinity, a complex composition, and a porous structure. Additionally, the annual production of RM is approximately 180 million tons [17]. China's comprehensive utilization rate of PG is approximately 40% [18], whereas that of red mud is less than 5% [19]. The accumulation of both materials in large quantities not only occupies a large amount of land resources but also tends to cause environmental contamination [20,21]. Due to the specific properties and structures of PG and RM, they have a certain adsorption capacity [22–24], but to improve their adsorption performance and safety in utilization, they must be modified.

Lanthanum (La) is a rare earth element with a high relative abundance, mainly found in the trivalent form with a special electronic layer structure, and these special structures make La highly chemically active and biocompatible; therefore, researchers have used La to modify zeolite [25], biochar [26], and CoFe_2O_4 nanocomposites [27] to improve the adsorption performance for As and P. However, relatively little research has examined the simultaneous adsorption of Cd and As on La-modified materials.

In this study, the raw materials PG and RM were utilized and transformed into the composite material L-PR through La impregnation. The objective was to investigate the impact of various factors, including dosage, pH, initial concentration, and adsorption time, on the efficacy of removing of Cd(II) and As(V) through batch adsorption experiments. Furthermore, our aim was to elucidate the potential mechanisms underlying Cd(II) and As(V) adsorption by L-PR and its passivation effect on soil contamination. Ultimately, our overarching goal was to provide a theoretical foundation and technical support for the remediation of water bodies and agricultural soils contaminated by Cd and As, as well as for the resourceful use of PG and RM.

2. Materials and Methods

2.1. Materials

Phosphogypsum (PG) was obtained from a phosphorus chemical company in Guizhou, China, and red mud (RM) was obtained from an aluminum plant in Guizhou, China. The chemical compositions of the two raw materials are presented in Table S1. The tested soil was collected from the topsoil layer (0–20 cm) of a paddy field (28°0'33" N, 113°19'25" E) in Liuyang City, Hunan Province, China. The basic physico-chemical properties of the soil are as follows: pH = 5.02, total Cd and total As concentration were 2.17 and 82.65 mg/kg, respectively, and the Cd and As concentrations of this soil were much higher than the screening value of the soil contamination risk of farmland soils. At pH ≤ 5.5, the limits for Cd and As are 0.3 and 30 mg/kg, respectively (*China Environmental Quality Standard GB 15618-2018*) [28]. The basic physico-chemical properties of the test soil are shown in Text S1, and the parameters are shown in Table S2. Lanthanum chloride heptahydrate ($\text{LaCl}_3 \cdot 7\text{H}_2\text{O}$, AR) and cadmium nitrate tetrahydrate ($\text{Cd}(\text{NO}_3)_2 \cdot 4\text{H}_2\text{O}$, AR) were supplied by Aladdin Biochemical Technology Co., Ltd., in Shanghai, China, and disodium arsenate heptahydrate ($\text{HAsNaO}_4 \cdot 7\text{H}_2\text{O}$, AR) was supplied by Sigma Au Sigma Oderich (Shanghai) Trading Co., Shanghai, China. The fundamental physical and chemical properties of the test materials are presented in Table S3.

2.2. Preparation of Adsorbents

Phosphogypsum (PG): PG was washed with ultrapure water (KNSY1016, Chengdu Aike Water Treatment Equipment Co., Ltd., Chengdu, China) to remove soluble impurities, filtered, subjected to vacuum drying in a DZF-6050 oven (Shanghai Yiheng Scientific Instrument Co., Ltd., Shanghai, China) at 80 °C, and then ground to 100 mesh. Red mud (RM): fresh Bayer RM was dried and ground to 100 mesh. Phosphogypsum red mud (PR): PG and RM were mixed in a 1:4 ratio, ultrapure water was added at a solid–liquid ratio of 1:20 and put into a magnetic stirrer (HSC-19T, Ningbo Qunan Experimental Instrument Co., Ltd., Ningbo, China) with thorough stirring, and the resulting mixture was centrifuged (Eppendorf5430r, Shanghai Jianling Information Technology Co., Ltd., Shanghai, China), dried, and ground to 100 mesh. Lanthanum-modified phosphogypsum red mud (L-PR): A certain amount of PR was placed into a beaker; 0.1 mol/L $\text{LaCl}_3 \cdot 7\text{H}_2\text{O}$ was added at a solid–liquid ratio of 1:20. The mixture was subsequently agitated on a magnetic stirrer for 5 h before being centrifuged and washed with ethanol. Finally, the samples were subjected to drying at a temperature of 80 °C and ground to 100 mesh.

2.3. Adsorption Experiments

$\text{Cd}(\text{NO}_3)_2 \cdot 4\text{H}_2\text{O}$ and $\text{HAsNaO}_4 \cdot 7\text{H}_2\text{O}$ were dissolved in ultrapure water to prepare stock solutions of Cd(II) and As(V), respectively, with a concentration of 1000 mg/L. These solutions were further diluted for use. The effects of different factors, including dosage (0.1–12 g/L), adsorption time (0–1440 min), pH (3–9), and initial concentration, were investigated. The composite solutions of Cd(II) and As(V) for the isothermal adsorption experiments were prepared as follows: the concentration of Cd(II) was held constant (1 mg/L), and the initial concentration of As(V) was varied (1–100 mg/L); the concentration of As(V) was kept constant (40 mg/L), and the initial concentration of Cd(II) was varied (1–100 mg/L). The concentrations of Cd(II) and As(V) used in all the adsorption experiments were 1 and 40 mg/L, respectively, except for the isothermal adsorption experiments. The filtrate was obtained by centrifugation at a uniform speed of 200 r/min for 24 h at ambient temperature, passed through a 0.45 µm filter membrane, and then detected by an inductively coupled plasma mass spectrometer (ICP-MS, ICAP RQ, Thermo Fisher Scientific, Waltham, MA, USA) and an atomic fluorescence spectrometer (AFS, AF-640A, Beijing Beifen Ruili Analytical Instrument (Group) Co., Beijing, China). The Cd(II) and As(V) concentrations were detected, and the adsorption experiments in this series were performed in 100 mL round-bottom centrifuge tubes. Each treatment was repeated three times.

The adsorption capacity (Q_e) [29] and removal rate (R) [30] were determined using the following equations:

$$Q_e = \frac{(C_0 - C_e)V}{m} \quad (1)$$

$$R = \frac{C_0 - C_e}{C_0} \times 100\% \quad (2)$$

Kinetic adsorption data were fitted with pseudo-first-order and pseudo-second-order kinetics models [31], while Cd(II)/As(V) adsorption by L-PR was simulated using Langmuir and Freundlich isotherm models [32].

$$\ln(Q_e - Q_t) = \ln Q_e - K_1 t \quad (3)$$

$$\frac{t}{Q_t} = \frac{1}{K_2 Q_e^2} + \frac{t}{Q_e} \quad (4)$$

$$\frac{C_e}{Q_e} = \frac{C_e}{Q_m} + \frac{1}{Q_m K_L} \quad (5)$$

$$\ln Q_e = \left(\frac{1}{n}\right) \ln C_e + \ln K_F \quad (6)$$

The initial and equilibrium concentrations of metal ions are represented by C_0 and C_e (mg/L), respectively. The mass of the adsorbent is denoted as m (g), while V (L) refers to the volume of the liquid. Q_t , Q_e , and Q_m (mg/g) denote the adsorption amount at reaction time t , the adsorption amount at equilibrium, and the maximum saturated adsorption, respectively. The time of the adsorption reaction is denoted as t (min). K_1 and K_2 refer to the pseudo-first-order and pseudo-second-order rate constants, respectively. K_L and K_F represent the Langmuir and Freundlich adsorption constants, respectively. And n signifies the Freundlich parameter indicating the adsorption strength.

2.4. Characterization

The surface morphology was analyzed using a scanning electron microscope (SEM, HITACHI/SU8600, Hitachi High-Technologies, Ltd., Tokyo, Japan) coupled with energy-dispersive X-ray spectroscopy (EDS, Oxford/ULTIM MAX40, Oxford Instruments Nanotechnology Tools Ltd., Tokyo, Japan), and the major components in the field of view were identified through energy spectral analyses. Specific surface area and pore size analyses were conducted using a Brunauer–Emmett–Teller (BET) analysis system (ASAP 2460 3.01, Mack Instruments, Norcross, GA, USA). The main crystal components were analyzed by X-ray diffraction (XRD; Rigaku Ultima IV, Rigaku Corporation, Tokyo, Japan). The chemical composition of the adsorbent was measured using X-ray fluorescence (XRF, ZSX Primus III+, Rigaku Corporation, Tokyo, Japan). Surface functional groups were identified using Fourier-transform infrared spectroscopy (FTIR, Nicolet 670, Nicolette Corporation, Madison, WI, USA) and X-ray photoelectron spectroscopy (XPS, Thermo Scientific K-Alpha Nexsa, Waltham, MA, USA). The isoelectric point and zeta potential of the adsorbent were determined under different conditions using a laser particle sizer (Zetasizer Nano ZS90, Malvern Panalytical, Malvern, UK).

2.5. Soil Incubation Experiments

The tested material and soil were thoroughly mixed in a beaker with 3% w/w deionized water added, stirred once a day, equilibrated for 1 week, and then transferred to a 25 °C, 70% RH incubator for incubation. Deionized water was replenished every 3 d during incubation using the weighing method to maintain the soil water content at 70% of the field holding capacity without the addition of passivator (Control, CK), and five parallels were established for each treatment. Sampling was performed after 55 d of incubation to determine the availability and fractions of As and Cd in the soil. The soil availability of Cd, reference [33]; the soil availability of As, reference [34]; the fractions of As and Cd in the samples were determined by the modified BCR sequential extraction method [35]. The

availability and fractions of As and Cd in the soil and the detailed procedure are described in Table S4.

2.6. Statistical Analysis

Excel 2010 (Microsoft Corp., Redmond, WA, USA) was used for data processing, and SPSS 26.0 (IBM Corp., Armonk, NY, USA) statistical analysis software was used for descriptive statistics, Pearson's correlation analysis, and one-way analysis of variance (ANOVA), with different lowercase letters showing key differences between treatments ($p < 0.05$). Adsorption kinetic and thermodynamic models were simulated using Origin 2018 (Origin Lab Corp., Northampton, MA, USA).

3. Results

3.1. SEM

The surface morphology of PG, RM, PR, and L-PR is shown in Figure 1a–d. These SEM images clearly show the surface morphology features of the four materials. PG is dominated by oblique crystals, the crystal structure is mainly rhombic, and the surface is relatively smooth with some irregular concave and convex structures and a small number of particles attached. RM consists of particles of different sizes with gaps between the particles, and the surface is somewhat rough and relatively disordered. After PG and RM were fully mixed, some fine particles can be seen attached onto the crystals with an irregular morphology interspersed with numerous flaky particles, and the surface is relatively rough (Figure 1a PR). After La modification, the surface of L-PR is obviously rough and fluffy, many flocculent materials appear, the particles are more loosely packed, and the pore space increases. Based on the results of energy-dispersive X-ray spectroscopy (EDS) (Figure S1), the main elements of the original PG are C, O, Ca, and S, and the contents of Al, Si, and P are relatively small, in addition to the presence of a very small amount of F, which was not detected after modification. The primary constituents of the original RM include C, O, Fe, Al, Si, and Ca, and the contents of Mg, Na, K, and S are relatively low. L-PR is predominantly composed of O, Ca, Fe, Al, Si, and La. It is evident that the successful loading of La onto the surface of PR has occurred.

3.2. N₂ Adsorption/Desorption Isotherm

The N₂ adsorption/desorption curves of each adsorbent are shown in Figure 1e. The adsorption of N₂ on RM, PR, and L-PR increases with increasing relative pressure, with the curve transitioning from a flat to a sharp increase and then a plateau, while the adsorption of PG remains essentially flat. The BET method was utilized for the determination of the specific surface area, pore volume, and pore size of the materials. The specific surface area and pore volume of PR and L-PR are significantly higher than those of PG and RM, as demonstrated in Table S3. Furthermore, a substantial increase in both the specific surface area and pore volume is observed after compositing. This behavior contradicts that of the average pore diameter; the specific surface area of the materials is dependent on the pore diameter, whereby smaller pore diameters result in larger specific surface areas. The decrease in the specific surface area and pore diameter of L-PR compared to PR is likely attributed to the increased particle size of PR caused by La loading onto its surface, which subsequently obstructed the pores. Moreover, the pore size distributions of the porous media were plotted (Figure 1f), and the pore types were analyzed; the pore size distribution is almost uniform, falling primarily in the range of 2–50 nm.

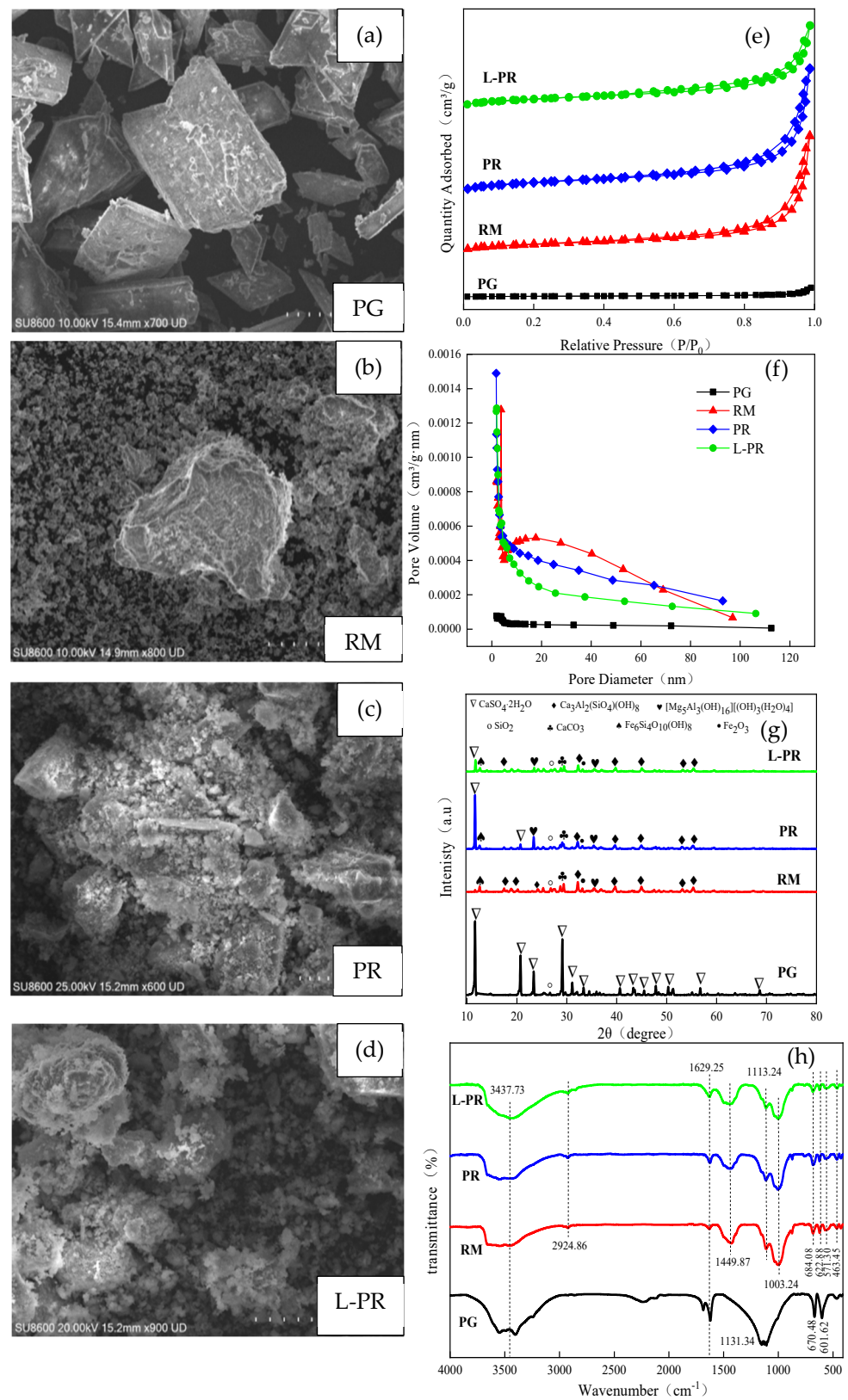


Figure 1. (a–d) SEM images of PG, RM, PR, and L-PR; (e) N₂ adsorption/desorption isotherms; (f) pore size distribution curves; (g) XRD patterns; and (h) FTIR spectra. Note: PG, phosphogypsum; RM, red mud; PR, phosphogypsum red mud; L-PR, lanthanum-modified phosphogypsum red mud.

3.3. XRD

The XRD pattern of PG, as depicted in Figure 1g, shows prominent diffraction peaks corresponding to $\text{CaSO}_4 \cdot 2\text{H}_2\text{O}$, indicating that the primary constituent of PG is $\text{CaSO}_4 \cdot 2\text{H}_2\text{O}$ with a minor presence of SiO_2 . RM mainly consists of bauxite residue, and the characterization results show that a variety of minerals coexist. The diffraction peaks of $\text{Ca}_3\text{Al}_2\text{SiO}_4(\text{OH})_8$, $\text{Fe}_6\text{Si}_4\text{O}_{10}(\text{OH})_8$ and $\text{Mg}_5\text{Al}_3(\text{OH})_{16}(\text{OH})_3(\text{H}_2\text{O})_4$ can be identified in the diffraction pattern of RM, and the diffraction peaks of CaCO_3 and Fe_2O_3 also appear in the diffraction pattern of RM. The composition of the physical phases is basically the same as the chemical composition in Table S1. Compared with those of the original material, no new peaks appear in the spectrum of the composite PR. After modification by La, the composition of the physical phase does not change significantly, but the characteristic peaks are significantly weakened, indicating that the crystallinity of the material decreases by the incorporation of La into the composite of RM and PG, and the diffraction peaks, especially the diffraction peaks of $\text{CaSO}_4 \cdot 2\text{H}_2\text{O}$, significantly change. Moreover, the diffraction peaks, XRF results, and EDS results of the composite PR indicate that La exists as amorphous lanthanum oxides or lanthanum hydroxides.

3.4. FTIR

The FTIR spectrum in Figure 1h exhibits two peaks at 3437.73 cm^{-1} and 1629.25 cm^{-1} , which can be attributed to the stretching vibration and bending vibration of hydroxyl groups (-OH) on the surface of the sample, respectively [36]. The intensity of the -OH peaks for PG is greater than that for RM, indicating that PG contains more crystalline water, while the crystalline water content decreases after the combination of PG with RM and modification with La. This decrease is not obvious after La modification, which may be mainly due to the loss of bound water in the structural framework during the compositing and modification process, which decreases the adsorption resistance of the raw materials and increases the diffusion of adsorbate molecules, thus increasing the adsorption capacity of PG and RM. The infrared sensitivity of SO_4^{2-} results in the prominent observation of a peak at 1131.24 cm^{-1} in PG, which corresponds to CaSO_4 . Additionally, the peaks at 610.62 cm^{-1} and 670.48 cm^{-1} can also be ascribed to SO_4^{2-} in the tetrahedral configuration [37]. Moreover, the response of these characteristic peaks is significantly weakened after complexation with RM, but the weakening is not obvious after modification by La. For RM, the C-H stretching vibration peak of alkoxy groups, observed at 2924.86 cm^{-1} [38], exhibits a weak sharp peak, which is further intensified through modification. The presence of carbonate compounds is indicated by the peak at 1449.87 cm^{-1} , which corresponds to the CO_3^{2-} stretching vibration [39,40]. However, this peak is weakened in PR and L-PR. The fingerprint regions of PR and L-PR have more characteristic peaks than that of PG, and the peaks in this region are more complicated. The peaks near 570 cm^{-1} and 690 cm^{-1} may be Fe-O, whereas the peaks around 622.88 cm^{-1} and 465.05 cm^{-1} may be Al-O; additionally, a strong and distinct peak at 1003.24 cm^{-1} could be ascribed to SiO_3^{2-} or SiO_4^{2-} [41]. The intensity of this peak is weakened by La modification. Due to the large covalent radius of La, when La replaces Si in the silica-aluminum tetrahedral skeleton of RM, it leads to an increase in the flexural vibration of Si-O bonds and a decrease in the bending vibration of Si-O-Si, suggesting the incorporation of La into the silica-oxygen tetrahedral skeleton [42]. These findings are corroborated by the crystalline peaks, such as those of calcium sulfate and silica aluminates, detected in the XRD analysis of PG and RM. The peaks present in both PG and RM are also present in L-PR, and these changes further confirm the complete fusion of PG and RM and the successful loading of La onto the composite.

3.5. Removal Rate of Cd(II)/As(V) before and after Adsorbent Modification

The removal rates of single Cd(II)/As(V) and binary Cd(II)/As(V) for each material are presented in Figure 2a and b, respectively. In the single system, L-PR exhibits removal rates greater than 97.57% for Cd(II) and 99.00% for As(V), while the removal rates of As(V) are significantly higher compared to PG, RM, and PR. Similarly, the removal rates of Cd(II) by L-PR are significantly higher than those of PG and RM, with no significant difference from PR. In the binary system, L-PR achieves removal rates of 98.37% for Cd(II) and 99.81% for As(V). Furthermore, As(V) is removed significantly more effectively than PG, RM, and PR; whereas Cd(II) shows a significant increase compared to PG and RM but not PR. In addition, the presence of As(V) enhances the removal efficiency of Cd(II) by PG and RM. These findings demonstrate that combining PG and RM substantially improves the removal efficacy of Cd(II), while La modification maintains high adsorption capacity for Cd(II) and significantly enhances As(V)'s elimination by PR. Therefore, considering their respective performance in removing both Cd(II) and As(V), L-PR was chosen as the test material in subsequent experiments.

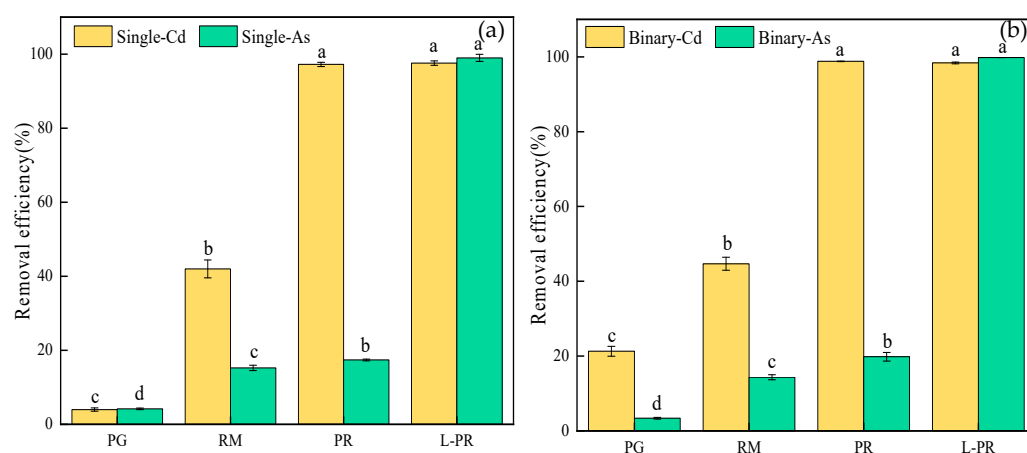


Figure 2. (a) Removal efficiency of Cd(II)/As(V) by PG, RM, PR, and L-PR in single system; (b) removal efficiency of Cd(II)/As(V) in binary system. Note: PG, phosphogypsum; RM, red mud; PR, phosphogypsum red mud; L-PR, lanthanum-modified phosphogypsum red mud; the different letters denote values are significantly different at $p < 0.05$.

3.6. Factors Affecting the Adsorption of Cd(II)/As(V)

3.6.1. Dosage of L-PR

The impact of the adsorbent dosage on the removal efficiency of Cd(II)/As(V) was investigated through an optimization process to determine the optimal adsorbent dosage. The experimental conditions were adjusted to include an initial Cd(II) concentration of 1 mg/L, an initial As(V) concentration of 40 mg/L, a temperature maintained at 25 °C, and an adsorption duration of 24 h. By varying the dosage of L-PR adsorbent (ranging from 0.1 g/L to 12.0 g/L), the effects on Cd(II)/As(V) removal were examined in detail. The obtained results are presented in Figure 3a–c. The figures demonstrate that an increase in L-PR dosage leads to the gradual augmentation of adsorption active sites, resulting in the enhanced removal of Cd(II) and As(V). However, due to the constant initial concentration of Cd(II) and As(V), the adsorption capacity gradually diminishes with higher L-PR dosage. Notably, as the L-PR dosage increases, there is a progressive rise in the quantity of active adsorption sites on its surface, leading to improved efficiency and reaching a saturation point when the amount of L-PR exceeds the critical value required for the complete adsorption of heavy metal ions. For instance, at a dosage of 1.0 g/L, the removal rates are 62.76% (single Cd), 52.79% (single As), 44.88% (binary As), and 99.42% (binary Cd). The impact of increasing the adsorbent dosage beyond a certain threshold on the removal rate and adsorption capacity of Cd(II) from the binary system is not significant, likely attributed to the presence of As(V), which enhances Cd(II) adsorption. At an adsorbent dosage of

4.0 g/L, high removal rates are achieved for single Cd, single As, and binary As at 97.87%, 99.45%, and 99.84%, respectively; further increases in L-PR dosage have minimal effect on the removal rate at this point. In conclusion, considering economic benefits, the optimal dosage of adsorbent is determined to be 4 g/L.

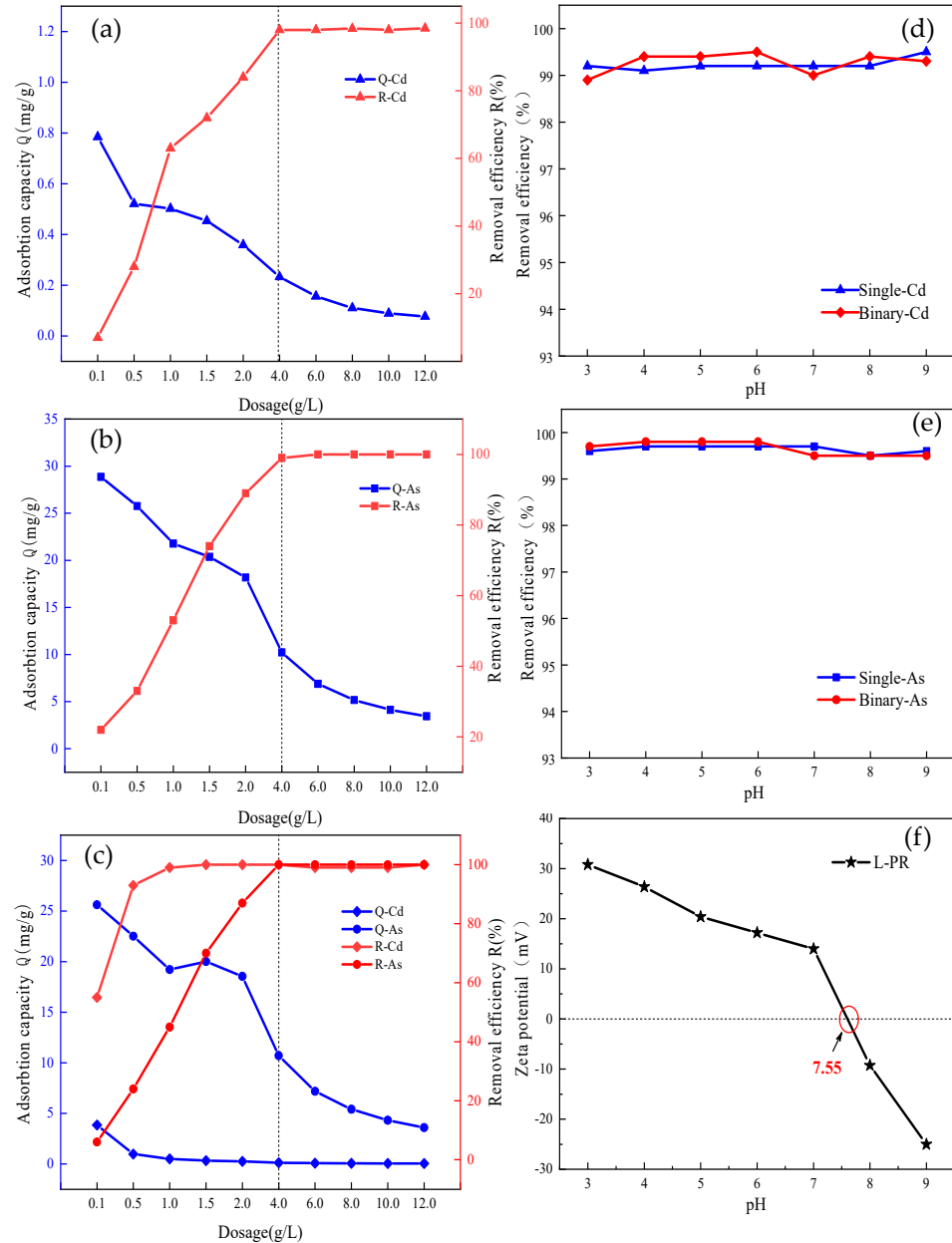


Figure 3. (a) Effect of L-PR dosage on single Cd adsorption; (b) effect of L-PR dosage on single As adsorption; (c) effect of L-PR dosage on binary Cd/As adsorption; (d) effect of pH on removal efficiency of single and binary Cd; (e) effect of pH on removal efficiency of single and binary As; (f) zeta potential of L-PR.

3.6.2. pH

The initial pH serves as a crucial indicator for determining the quantity of metal adsorbed by a material. The initial pH has no impact on the removal efficiency of Cd(II)/As(V) by L-PR. Remarkably, both Cd(II) and As(V) removals exhibit high efficiency, reaching up to 99% within a wider pH range of 3.0~9.0 (Figure 3d,e). Figure 3f illustrates the variation in the zeta potential of L-PR under different pH conditions. The isoelectric point (pH_{pzc}) of L-PR is 7.55, leading to the generation of a cationic surface when the pH value falls below

this threshold due to protonation by H^+ ions. This facilitates electrostatic attraction between L-PR and arsenite or arsenate, while the adsorption of As(V) by L-PR is primarily regulated by electrostatic adsorption. However, in theory, the protonation on the L-PR surface at a lower pH would theoretically hinder the binding of cationic Cd(II) to the L-PR surface due to charge repulsion. Nevertheless, experimental results demonstrate that the removal efficiency of Cd(II) by L-PR still reaches 99%. Therefore, it can be concluded that electrostatic attraction does not play a dominant role in the adsorption of immobilized Cd(II) by L-PR within this pH range. Furthermore, L-PR maintains a high removal efficiency of Cd(II)/As(V) at a pH > 7.55 due to the deprotonation and negative charge on its surface. Hence, within this pH range, the adsorption of Cd(II) occurs through electrostatic attraction, while the adsorption of As(V) is less influenced by electrostatic attraction. In conclusion, L-PR exhibits suitability across a wide pH range which enhances its practical applicability.

3.6.3. Adsorption Isotherm

The adsorption behavior of Cd(II)/As(V) on L-PR was examined at 25 °C, and the collected data were analyzed using the Langmuir and Freundlich models. The results are illustrated in Figure 4, along with the fitting parameters provided in Table 1. The Freundlich equation is commonly considered as an empirical model that assumes multilayer adsorption on a nonhomogeneous surface. The Langmuir model, in contrast, assumes monolayer adsorption on a homogeneous surface without any intermolecular interactions between the adsorbed molecules at adjacent positions. In other words, adsorption takes place exclusively on the outer surface of the adsorbent. The correlation coefficients (R^2) indicated distinct L-PR adsorption mechanisms for Cd(II) and As(V). The adsorption of Cd(II) was found to be more consistent with the Freundlich model, as evidenced by R^2 values of 0.955 (single) and 0.951 (binary), while the adsorption of As(V) was better fit with the Langmuir model, supported by R^2 values of 0.969 (single) and 0.985 (binary). The results indicated that the adsorption of Cd(II) by L-PR is likely to occur through non-homogeneous multilayer adsorption, while As(V) adsorption predominantly takes place via homogeneous monolayer adsorption. The saturation adsorption capacities (Q_{max} values) for single system Cd(II) and binary system As(V) were determined as 12.508 mg/g and 10.654 mg/g, respectively. The Langmuir adsorption constant, K_L , quantifies the affinity between the adsorbent and the adsorbate; a higher value signifies a stronger affinity. The Freundlich adsorption constant, K_F , quantifies the adsorption capacity of the adsorbent. The affinity and adsorption capacity of L-PR for As(V) were found to be superior to those for Cd(II) in all systems. However, in the binary system, the affinity and adsorption capacity of L-PR for As(V) decreased, while there was a slight increase in its affinity and adsorption capacity for Cd(II). This observed phenomenon can be ascribed to co-adsorption where the components mutually interfere with each other. In addition, the value of $0 < 1/n < 1$ in the Freundlich model indicated that the inhomogeneous surface of L-PR favors the adsorption of Cd(II) and As(V).

Table 1. Parameters of Cd(II)/As(V) adsorption calculated based on the Freundlich and Langmuir models.

Metal Types	Systems	Langmuir Model			Freundlich Model		
		Q_{max} (mg/g)	K_L (L/mg)	R^2	K_F (mg/g)	$1/n$	R^2
Cd(II)	Single	18.904	6.19×10^{-3}	0.740	0.888	0.141	0.955
	Binary	14.925	0.205	0.859	1.944	0.631	0.951
As(V)	Single	12.508	2.288	0.969	5.777	0.330	0.728
	Binary	10.654	1.191	0.985	4.163	0.356	0.731

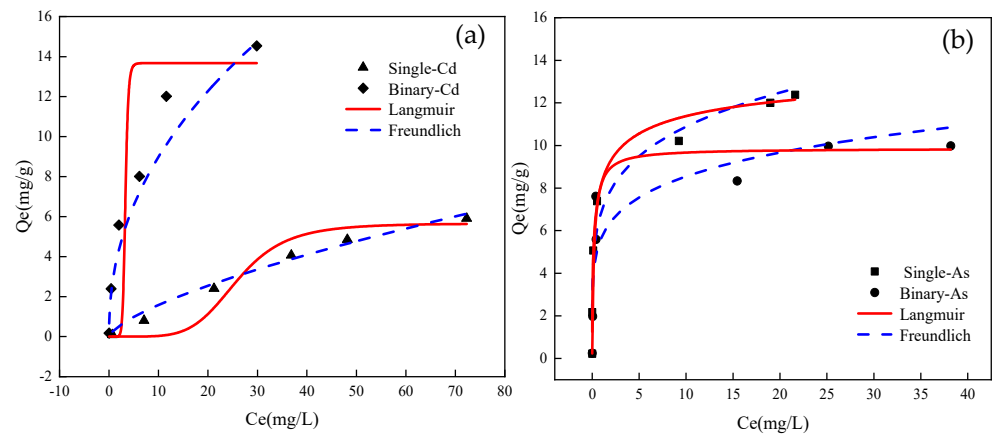


Figure 4. Langmuir and Freundlich isotherms for the adsorption of (a) Cd(II) and (b) As(V) by L-PR.

3.6.4. Adsorption Kinetics

The adsorption kinetics of Cd(II)/As(V) by L-PR were modeled using the pseudo-first-order and pseudo-second-order kinetic models (Figure 5), and the relevant fitting parameters are shown in Table 2. The fitting results revealed that the adsorption processes of Cd(II) and As(V) by L-PR were consistent with the pseudo-first-order and pseudo-second-order kinetic models ($R^2 > 0.99$) in two systems. The calculated equilibrium adsorption capacities Q_e were 0.336 (single Cd), 0.373 (binary Cd), 7.851 (single As), and 8.174 (binary As) mg/g, which are very close to the experimental values of 0.333 (single Cd), 0.373 (binary Cd), 7.198 (single As), and 8.163 (binary As) mg/g. The adsorption rates of both Cd(II) and As(V) by L-PR exhibited an initial rapid phase, as depicted in Figure 5, followed by a gradual decrease until reaching adsorption equilibrium. Furthermore, a decreased K_2 value signifies a prolonged duration for adsorption to achieve equilibrium. Compared to single adsorption, the adsorption rates of both Cd(II) and As(V) were significantly enhanced in the binary system; equilibrium was achieved within approximately 180 min for both systems, with the rapid adsorption of As(V) occurring within just 20 min and exhibiting a remarkable removal rate of 93.21%. In contrast, in the single system, As(V) adsorption reached equilibrium in approximately 6 h, and Cd(II) adsorption reached equilibrium in a relatively long time of approximately 18 h. This indicates that the presence of both Cd(II) and As(V) results in a shorter time to achieve removal equilibrium compared to their single systems, with chemical adsorption being the dominant mechanism.

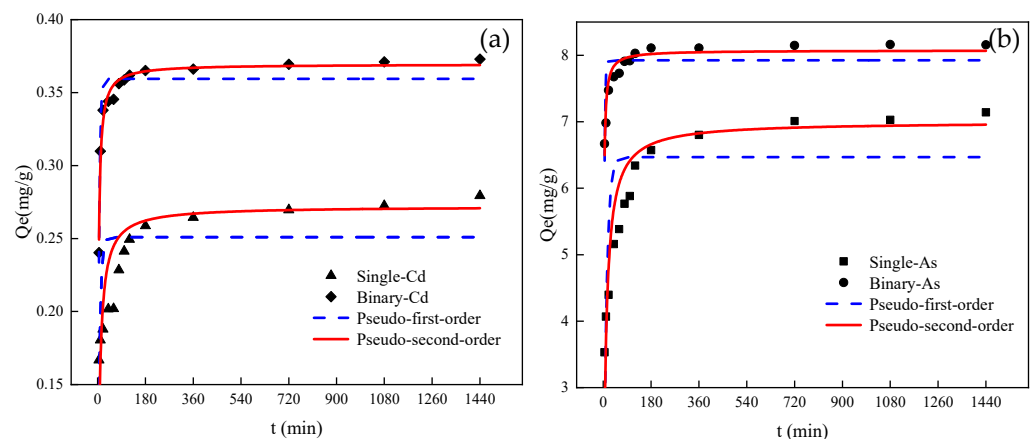


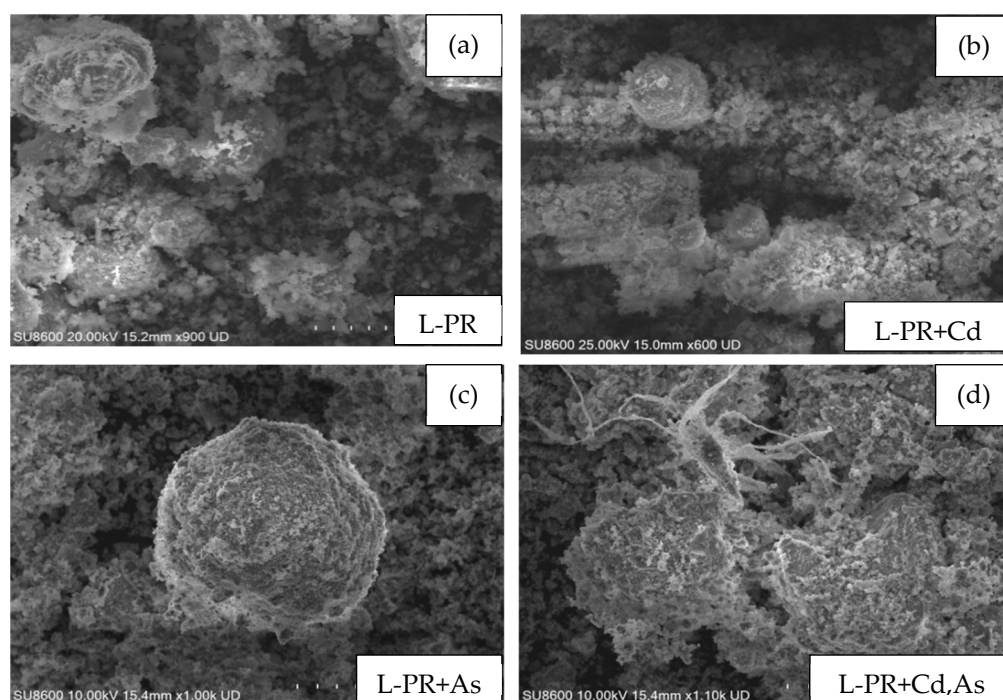
Figure 5. Adsorption kinetics of (a) Cd(II) and (b) As(V) by L-PR.

Table 2. Pseudo-first-order and pseudo-second-order kinetics fitting results of Cd(II) and As(V).

Metal Types	Systems	Pseudo-First-Order Kinetic			Pseudo-Second-Order Kinetic		
		Q_e (mg/g)	K_1 (1/h)	R^2	Q_e (mg/g)	K_2 (g/mg/h)	R^2
Cd(II)	Single	0.152	0.0027	0.993	0.336	0.0737	0.996
	Binary	0.035	0.0387	0.584	0.373	0.6961	0.999
As(V)	Single	3.270	0.0029	0.879	7.851	0.0048	0.996
	Binary	0.370	0.0037	0.646	8.174	0.0576	0.999

3.7. Possible Mechanism of Adsorption of Cd(II)/As(V) by L-PR

The SEM images in Figure 6a–d show the surface morphology of L-PR before and after the adsorption of Cd(II) and As(V). Following the adsorption process, the previously evacuated and flocculated surface of L-PR becomes more compact and dense, particularly in the single systems. Notably, the adsorption of As(V) by L-PR is more pronounced compared to that of Cd(II) in the single system. Additionally, it is worth highlighting that the presence of ribbon-like materials observed after Cd(II)/As(V) adsorption by L-PR may be due to complex formation between Cd(II) and As(V) on its surface.

**Figure 6.** (a–d) SEM images of L-PR before and after Cd(II)/As(V) adsorption.

A comparison of the XRD patterns of L-PR before and after Cd(II)/As(V) adsorption is presented in Figure 7. The $\text{CaSO}_4 \cdot 2\text{H}_2\text{O}$ peak is observed at 11.75° , while the $\text{Mg}_5\text{Al}_3(\text{OH})_{16}(\text{OH})_3(\text{H}_2\text{O})_4$ peak appears at 23.47° following the mono-adsorption of Cd(II). However, the peaks corresponding to mono-adsorbed As(V) and Cd(II)/As(V) disappear completely after co-adsorption. On the basis of these results, Ca^{2+} , Mg^{2+} , and Al^{3+} may be involved in ion exchange with Cd(II)/As(V).

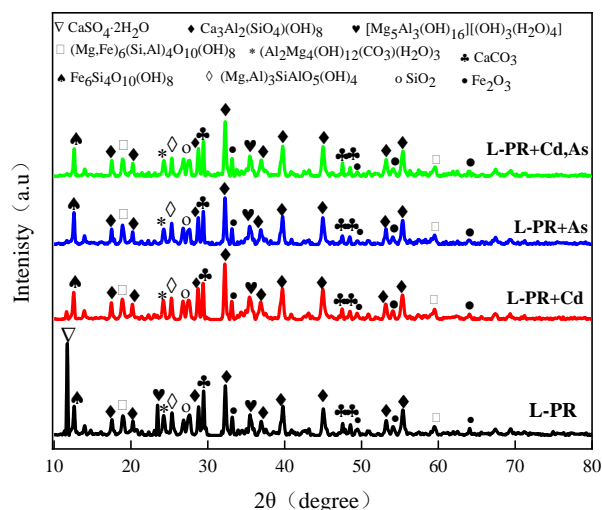


Figure 7. XRD patterns of L-PR before and after Cd(II)/As(V) adsorption.

According to the FTIR spectra before and after adsorption, as illustrated in Figure 8, the peaks at 3437.73 cm^{-1} reveal a reduction in intensity following the adsorption of Cd(II)/As(V) by L-PR. Furthermore, these peaks undergo a shift towards 3460.54 cm^{-1} upon the adsorption of Cd(II) alone by L-PR, 3458.43 cm^{-1} upon the adsorption of As(V) alone, and they finally settle at 3456.45 cm^{-1} following the simultaneous adsorption of Cd(II)/As(V). This phenomenon can be attributed to the broadening effect caused by the O-H stretching vibration on the overlapping flat peaks observed at 3437.73 cm^{-1} . After the adsorption of Cd(II) and As(V) alone, the peak associated with the C-H stretching vibration of alkoxy groups at 2924.86 cm^{-1} weakens and shifts, eventually disappearing completely upon the adsorption of Cd(II)/As(V), indicating the involvement of surface L-PR alkoxyates in both Cd(II) and As(V) adsorption. The CO_3^{2-} stretching vibration peak near 1449.87 cm^{-1} shifts to near 1428 cm^{-1} after the mono-adsorption of Cd(II) and co-adsorption of Cd(II)/As(V) and becomes sharp after co-adsorption, indicating that Cd(II) exchanges with carbonate cations to further form a precipitate. Moreover, the absorption peak at 1003.24 cm^{-1} for L-PR shows no significant change after the mono-adsorption of Cd(II), while the peak becomes narrower after mono-adsorbing As(V) and co-adsorbing Cd(II)/As(V), suggesting that La enters the silica–oxygen tetrahedron to participate in the adsorption of As(V), with which it may form complexes.

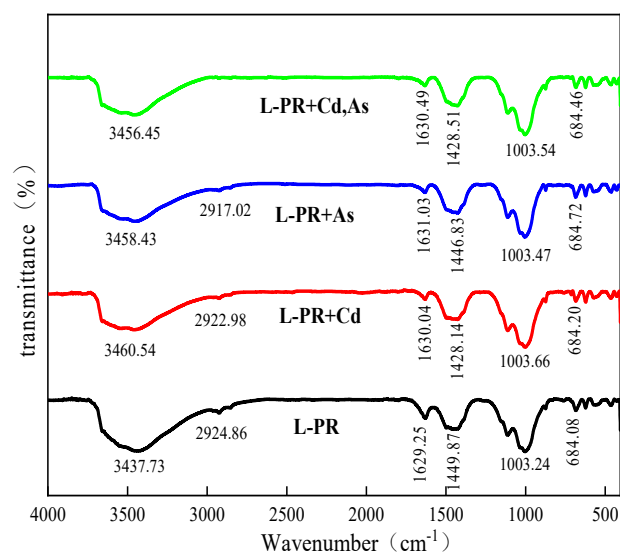


Figure 8. FTIR spectra of L-PR before and after Cd(II)/As(V) adsorption.

To gain a deeper understanding of the Cd(II)/As(V) adsorption mechanism on L-PR, a further XPS analysis was conducted to investigate the changes in functional groups on L-PR (Figure 9a–c). The presence of La 3d in the full XPS spectrum of L-PR further confirms that La was loaded onto the surface of PR. The adsorption of Cd(II)/As(V) was followed by the appearance of new characteristic peaks: the presence of Cd 3d (400.11 eV) and As 3d (44.12 eV) peaks confirms the successful adsorption of Cd(II) and As(V); moreover, the Ca 2p peak was significantly weakened, suggesting that the adsorption was related to ion exchange, which was also confirmed by the XRD and FTIR results.

Figure 9b shows the high-resolution spectra of O 1s prior to and subsequent to the adsorption process involving Cd(II)/As(V) on L-PR. PR is impregnated with elemental La, and the surface of L-PR exhibits characteristic peaks corresponding to metal oxides (Figure S2). This observation suggests that La is loaded onto PR in the form of metal oxides, which aligns with the XRF results. Moreover, the relative content of metal oxides decreases from 9.59% to 2.87% and 4.15%, while that of H-O increases from 90.41% to 97.13% and 95.85%, after adsorbing Cd(II) and As(V), respectively, on L-PR, suggesting that metal oxides, i.e., La-O, were involved in adsorbing Cd(II) and As(V). Notably, three peaks observed at 529.75, 530.99, and 532.75 eV after the co-adsorption of Cd(II)/As(V) can be attributed to As-O, H-O, and O in Cd-O, respectively. The involvement of L-PR in the adsorption process during Cd(II)/As(V) co-adsorption is worth mentioning, as evidenced by the decrease in the relative proportion of H-O from 90.41% to 65.69%. Cd(II) and As(V) can interact with H-O, leading to the substitution of H-O by Cd-O and As-O, respectively. This suggests the formation of ternary complexes during co-adsorption, which accord with the SEM results.

The C 1s spectra (Figure 9c) demonstrate significant changes in the binding energies of C=O/C-O, O-C=O, and CO_3^{2-} after the adsorption of Cd(II)/As(V); specifically, there is a shift towards higher binding energy for CO_3^{2-} following Cd(II) adsorption, resulting in a decrease in relative content from 4.50% to 2.49% (single) and 1.07% (binary), respectively. This indicates that CO_3^{2-} sites are occupied during adsorption, probably forming CdCO_3 with Cd(II) and contributing less to As(V) adsorption.

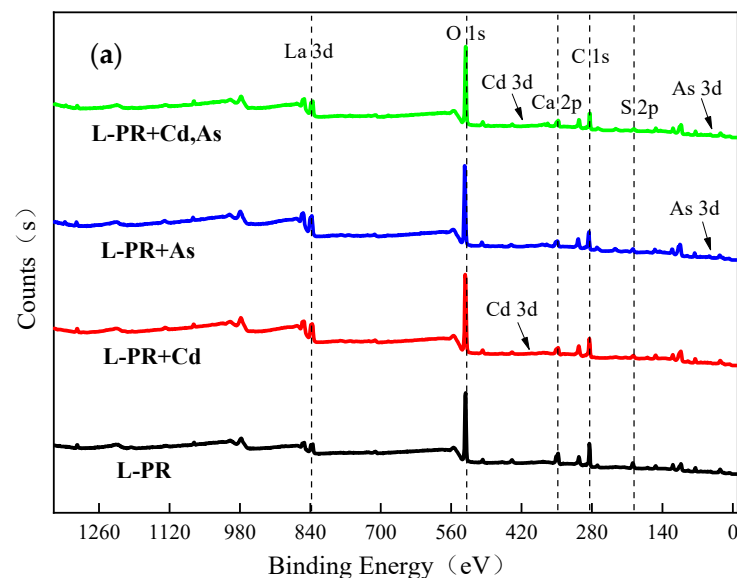


Figure 9. Cont.

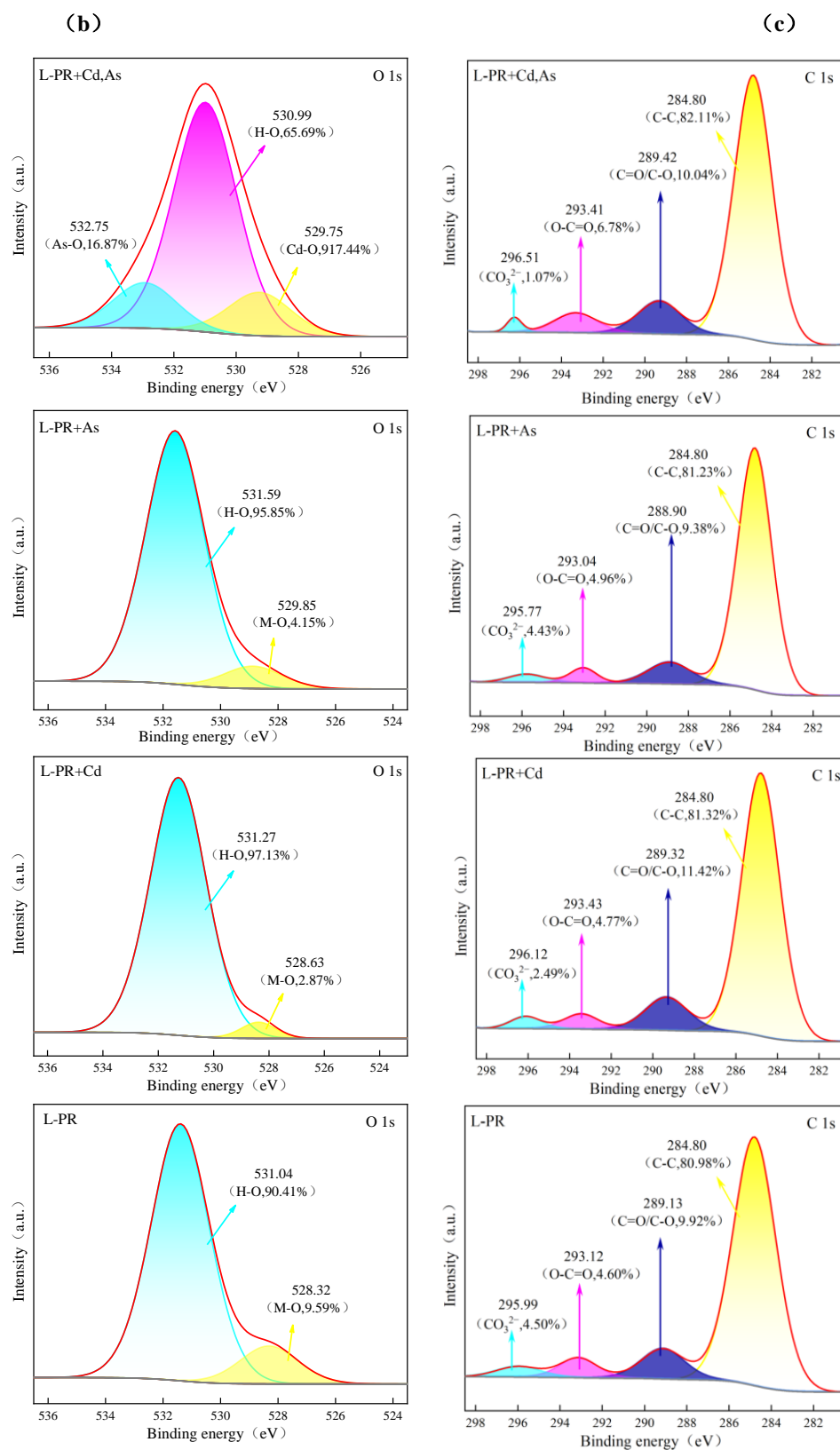


Figure 9. (a) XPS spectra of L-PR before and after Cd(II)/As(V) adsorption; (b) O 1s spectra of L-PR before and after Cd(II)/As(V) adsorption; (c) C 1s spectra of L-PR before and after Cd(II)/As(V) adsorption.

The split-peak fit of the Cd 3d orbitals (Figure S3) shows that Cd²⁺ accounts for 32.80% and Cd-O for 67.20% in the single system, while Cd²⁺ accounts for only 7.14% in the binary

system. Additionally, the As 3d spectra (Figure S4) reveal that approximately 70% of arsenic exists as As(V), while approximately 30% is present as As(III) in two systems. This suggests that ion exchange and complexation mechanisms enhance the adsorption of individual Cd(II) by L-PR, whereas the introduction of As(V) promotes the formation of Cd(II)/As(V) complexes. Moreover, As(V) adsorption may involve electron transfer, and the effect of Cd(II) addition on As(V) adsorption is not significant.

3.8. Effects of Various Treatments on As and Cd Availability and Fractions in Soil

3.8.1. Availability of Cd and As

The impacts of the various treatments on the soil availability of Cd and As are illustrated in Figure 10. In comparison to CK, the impact of PG on available Cd in soil is negligible. However, RM, PR, and L-PR significantly decrease the concentration of available Cd. The stabilizing effect of L-PR on Cd is notably superior to that of RM and PR, resulting in an 86.01% reduction in available Cd concentration in soil. Similarly, while the effect of PG on available As concentration remains almost unchanged, it is significantly higher in the RM and PR treatments. The application of L-PR reduces the available As concentration by 27.80%. Similarly, the impact of PG on available As concentration remains nearly unchanged in the PG treatment, while it is significantly elevated in the RM and PR treatments. Moreover, a reduction of 27.80% in available As concentration is observed in the L-PR treatment compared to CK. In conclusion, L-PR shows pronounced efficacy in reducing the toxicity caused by Cd and As, concurrently reducing their bioavailability.

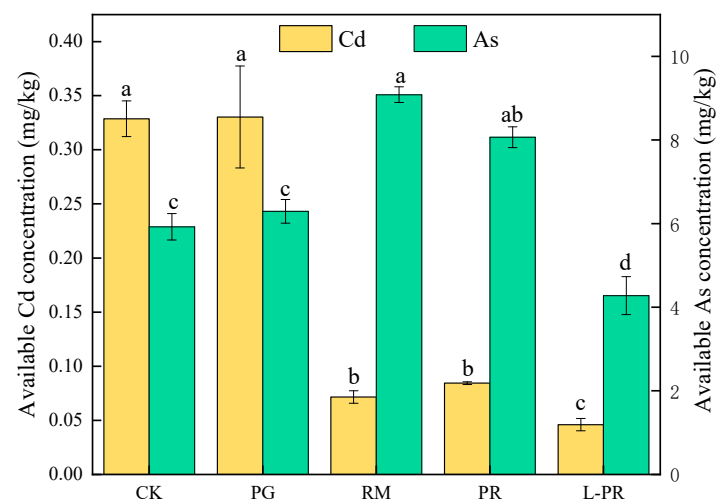


Figure 10. Available Cd and As concentrations in soil under different treatments. Note: CK, control; PG, phosphogypsum; RM, red mud; PR, phosphogypsum red mud; L-PR, lanthanum-modified phosphogypsum red mud; the different letters denote values are significantly different at $p < 0.05$.

3.8.2. Fractions of Cd and As

The morphology and fractions of heavy metals in soil are critical factors influencing their bioavailability. In order to gain a comprehensive understanding of the impact of L-PR on the changes in the morphological distribution of metals in soil and evaluate their levels of stabilization, the BCR sequential extraction of As and Cd in soil was carried out. As shown in Figure 11, the results of BCR continuous extraction indicated that the fraction of Cd in Cd-As complex-contaminated soil was mainly dominated by the residual (F4), which accounted for 51.67% of the total fractions concentrations, followed by the acid-soluble (F1) and reducible (F2), and the oxidizable (F3) accounted for a smaller proportion. Compared with CK, the application of L-PR reduces Cd acid-soluble F1 in soil, reducible F2, and oxidizable F3 concentrations, especially acid-soluble F1 and reducible F2, which decreased by 8.53% and 5.71%, respectively, while increasing the concentrations of residual F4 by 29.31%; for As, the highest proportion of the total fractions concentration is residual F4, which is as high as 85.75%, followed by reducible F2 and oxidizable F3, and the

lowest is acid-soluble F1, which is only 0.52%, which was hardly extracted by the BCR sequential extraction, indicating that most of the As in this Cd-As complex-contaminated soil existed in the form of immobilized fractions, and the Cd and As mobility is weak, and the concentrations of reducible and oxidizable As were reduced by 2.55% and 4.08%, respectively, and residual As was elevated by 6.56% under the L-PR treatment compared with that of CK, and the effect on the weakly acid-soluble As is not obvious. In conclusion, the addition of L-PR to soil can reduce the bioavailability of Cd and As in soil and induce the transformation of non-stable Cd/As to the more stable residual.

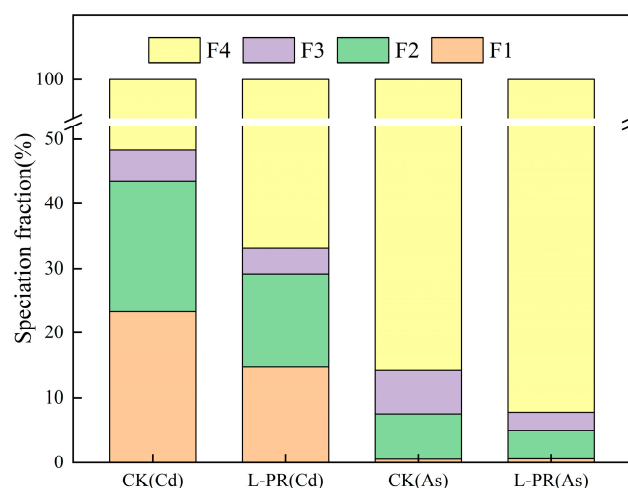


Figure 11. Fractions of Cd and As in soil under CK and L-PR treatments.

4. Discussion

4.1. Properties of L-PR

The SEM-EDS, BET, XRD, XRF, FTIR, and XPS characterization results showed that the combination of PG with RM and subsequent modification with La not only neutralized the pH of the raw material but also improved both its structure and composition. Structurally, the concave and convex bulk crystal structure of PG provided attachment points for the granular RM, which made its surface rougher. After La loading, the surface of L-PR was rough and fluffy, many flocculent materials appeared, and the particles were more loosely stacked (Figure 1 L-PR). Moreover, the specific surface area and pore volume obviously increased, the pore diameter became smaller (Table S3), and the diameters of almost all the pores were uniformly distributed in the range of 2 nm to 50 nm (Figure 1b). These results suggest that L-PR is a mesoporous material with a mineral surface and adsorption capacity [43], thereby contributing to the enhanced adsorption of heavy metals. In terms of composition, the combination of CaSO_3 , the main component of PG, and Al_2O_3 , Fe_2O_3 , SiO_2 , and MgO in RM was observed (Table S1); relevant studies have confirmed that Ca, Al, Mg, and Fe ions can adsorb Cd(II) and As(III) via ion exchange [44,45]. Moreover, Li et al. demonstrated the presence of oxygenated functional groups associated with La and provided evidence for the involvement of La-O in the adsorption process of As(V) [26]; in addition, functional groups such as H-O and Si-O were modified. Furthermore, Wu et al. indicated that the activation of more oxygenated functional groups on adsorbent materials was favorable for the adsorption of Cd and Pb [46].

4.2. Adsorption Behavior of Cd(II)/As(V) on L-PR

The removal efficiency of Cd(II) by L-PR exceeded 97.57%, while the removal efficiency of As(V) surpassed 99.00% (Figure 2). In contrast, the removal of Cd(II) and As(III) by pyrite-modified biochar (PMB) only achieved a removal range of 70.00–80.00% for Cd(II) and As(III) [47]. Nitrogen-doped biochar (NBC), however, demonstrated the highest removal rates for Cd(II) and total arsenic As(T), reaching 89.00% and 94.00%, respectively [48]. On the other hand, natural ferromanganese nodules removed approximately 83.60% of total

arsenic As(III, V) [49]. Notably, L-PR exhibited superior adsorption performance for Cd(II) and As(V), with its adsorption capacity remaining unaffected by pH. The surface of L-PR was protonated and positively charged at $\text{pH} < 7.55$, thereby enhancing the electrostatic attraction between the adsorbent surface and As(V). This observation is consistent with previous experimental findings on the adsorption of As(V) by other La-modified materials. The surface of Fe-Mn-La-impregnated biochar composites also displayed a positively charged surface due to protonation at a low pH, and this material was used to adsorb As(V) by electrostatic action in reactions with arsenite or arsenate [50]. Furthermore, in acidic and neutral conditions, La^{3+} ions leached from Fe-La composite oxides could react with As(V) to form the insoluble precipitate LaAsO_4 [51]. At $\text{pH} > 7.55$, L-PR maintained a high removal efficiency of Cd(II)/As(V). Although the solution conditions were unfavorable for the electrostatic adsorption of As(V), other chemical interactions occurred, and when the pH of the initial solution was higher than the pH_{pzc} , arsenate was released into the solution by replacing -OH on the surface, and ligand exchange occurred during the adsorption process [50,52] due to the deprotonation of -OH and -COOH groups at higher pH values, which promotes complexation with metal ions [53]. The removal of Cd(II) by modified biochar also increased with rising solution pH, and Cd(II) readily generated $\text{Cd}(\text{OH})_2$ precipitates [54]. The results from fitting the kinetic and adsorption isotherm models for Cd(II)/As(V) showed that the adsorption of Cd(II) by L-PR exhibited characteristics of nonhomogeneous adsorption in multimolecular layers. The adsorption process of Cd(II)/As(V) was dominated by chemisorption, and the time required to reach removal equilibrium for co-adsorption was shorter than that for mono-adsorption. The disparity in the initial adsorption rate can be ascribed to the discrepancy in the affinities of the adsorbents towards the metal ions [55]. Therefore, when Cd(II)/As(V) coexisted, they mutually promoted the affinity of L-PR for each other, and synergistic adsorption occurred.

4.3. Main Mechanism of Cd(II)/As(V) Adsorption by L-PR

The mechanism of adsorption of heavy metals by adsorbents involves a combination of electrostatic attraction, ion exchange, complexation, and precipitation/coprecipitation [56,57]. The SEM and XRD results revealed that after adsorbing Cd(II)/As(V), although no new distinctive peaks were generated, changes in surface structure and physical phase can be observed. Additionally, the $\text{CaSO}_4 \cdot 2\text{H}_2\text{O}$ and $\text{Mg}_5\text{Al}_3(\text{OH})_{16}(\text{OH})_3(\text{H}_2\text{O})_4$ peaks were significantly weakened, which is similar to the results for adsorbing Cd(II) and As(V) by other mineral-based adsorbents [6,58]. Consequently, it can be inferred that ion exchange occurred between Ca^{2+} , Mg^{2+} , Al^{3+} , and Cd(II)/As(V). The FTIR, O 1s, and C 1s spectral results showed that -OH, La-O, and CO_3^{2-} were engaged in adsorbing Cd(II)/As(V). The appearance of hydroxyl groups in As-OH or Cd-OH indicates that the oxygen atom on -OH may coordinate with Cd(II)/As(V) [13]. Additionally, La-involved silica-oxygen tetrahedra are involved in the adsorption of As(V), forming complexes [42,51]. Furthermore, La-O is transformed into La-OH, leading to the precipitation of $\text{Cd}(\text{OH})_2$ with Cd(II) and the formation of complexes with As(V). Zhang et al. found that Fe-La composite oxides and As(V) formed bidentate binuclear (BB) or monodentate mononuclear (MM) complexes [51]. CO_3^{2-} changed after the adsorption of Cd(II), suggesting that Cd(II) exchanged with cations in carbonates to further form precipitates. This mechanism is consistent with the findings reported by Cai et al., who studied the removal of Cd(II) by NaOH-EtOH modified biochar [54]. After the co-adsorption of Cd(II)/As(V), Cd(II) and As(V) interacted with H-O, and substitution occurred to form Cd-O and As-O. It was deduced that ternary complexes were formed upon co-adsorption. Liu et al. showed that Fe-P-Cd ternary complexes were formed in the P and Cd co-adsorption system [59]. Wu et al. found that Fe-As-Cd ternary complexes formed upon the co-adsorption of Cd(II)/As(V) on magnetic biochar [60]. Su et al. found that As(V) and Cd(II) can promote each other's adsorption at the interface of acicular ferrite by forming a ternary complex (Fe-As-Cd) when they coexist [58]. We can summarize the mechanism of adsorption of L-PR for Cd(II)/As(V) as illustrated in Figure 12: (1) Electrostatic attraction: There is an attractive force between the

protonated and positively charged L-PR surface and As(V) when $\text{pH} < \text{pH}_{\text{pzc}}$, and there is an attractive force between the deprotonated and negatively charged L-PR surface and Cd(II) when $\text{pH} > \text{pH}_{\text{pzc}}$. FTIR analysis confirmed that Cd(II)/As(V) adsorption involves alkoxy C=H groups on L-PR, which implies the existence of electrostatic attraction in these adsorption processes. (2) Ion exchange: The XRD, FTIR, and XPS results revealed that the Ca^{2+} content decreased after the L-PR adsorption of Cd(II)/As(V), and the XRD results also showed that Mg^{2+} and Al^{3+} ions were involved in the adsorption process after modification. (3) Complexation: The FTIR and XPS analyses verified the presence of functional groups, specifically -OH and La-O, in the adsorption process. These functional groups formed complexes with Cd(II)/As(V) in the mono-adsorption systems and ternary complexes with Cd(II)/As(V) in the co-adsorption system. (4) Precipitation: The FTIR and XPS results confirmed the involvement of CO_3^{2-} and La-O in the adsorption of Cd(II), implying the formation of insoluble precipitates such as CdCO_3 and $\text{Cd}(\text{OH})_2$.

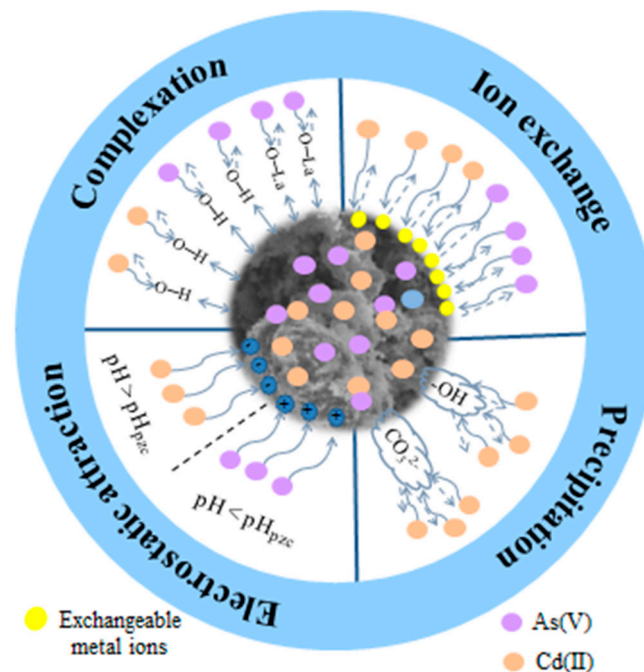


Figure 12. Schematic illustration of potential mechanisms for adsorption of Cd(II)/As(V) by L-PR.

4.4. Applicability of L-PR in Cd-As Complex-Contaminated Soil

In this study, L-PR significantly reduced the concentrations of available Cd and As in soil by 86.01% and 27.80%, respectively, compared to CK. The removal of Cd and As in soil by L-PR was lower than in aqueous solution, which may be due to the more complex soil environment and the low ionic mobility in soil [61], especially the removal of As in soil that was much lower than the results of adsorption tests in aqueous solution, but the removal rate of As in soil by L-PR was higher compared to other modified materials. For example, Li et al. found that the addition of 3% zeolite-modified nano-zero-valent iron reduced the effective As of Cd-As complex-contaminated soil by 17.10% [62]; Wu showed that the addition of calcium-based magnetic biochar (Ca-MBC) to Cd-As-contaminated soils reduced the effective As concentration by 12% [63]. Combined with BCR sequential extraction fractions analysis, we concluded that L-PR treatment had the effect of reducing the bioavailability and transport of Cd and As in soil. The addition of L-PR resulted in a significant reduction in the percentage of acid-soluble Cd and reducible Cd and an increase in residual Cd; Li et al. pointed out the weak acid dissolved state F1 and reducible state F2 in the effectiveness of Cd in soil [63–65]. Meanwhile, it is evident that the concentrations of reduced and oxidizable As decreased while the residual As increased, aligning with the findings reported by Ainiwaer et al. in their study on immobilizing As in Cd-As

complex-contaminated soil using seafoam-modified nano-zero-valent iron (SEP-nZVI) [66], which is attributed to the fact that it is L-PR that can promote the conversion of Cd/As in an unstable state to Cd/As in a stable state in the soil through electrostatic attraction, ion exchange, complexation, precipitation, and so on. Sun et al. found that seafoam in modified materials can fix Cd through electrostatic adsorption [67]. In addition, several studies indicated that the surface reaction of passivated materials for fixing Cd/As in soils is similar to the adsorption mechanism in aqueous solution [62,66,68].

5. Conclusions

In this paper, industrial by-products PG and RM were utilized as raw materials to improve their adsorption properties for Cd and As by lanthanide modification. La-O was successfully attached onto the PR structure through XRF and XPS analyses. The results of adsorption experiments demonstrated that the removal efficiency of L-PR for Cd(II) was more than 97.57%, and the removal efficiency of As(V) was more than 99.00%. The analysis of various models revealed a favorable correspondence between the pseudo-second-order kinetic model and the adsorption data of Cd(II) and As(V). Moreover, Cd(II) exhibited conformity to the Freundlich model, while As(V) adhered to the Langmuir model. The adsorption mechanism of Cd by L-PR was mainly found to involve a combination of ion exchange, precipitation, and complexation, while the adsorption of As mainly involved a combination of ion exchange and complexation based on XRD, FTIR, and XPS analyses. Soil cultivation experiments further confirmed that L-PR significantly reduced the available Cd and As concentrations in soil and could induce the transformation of unstable Cd/As to the more stable residual. Overall, L-PR not only effectively removed Cd(II) and As(V) from aqueous solutions but also simultaneously immobilized Cd and As in contaminated soil, which provides a good prospect for the management of Cd and As composite contamination in farmland soils that merits further investigation and evaluation.

Supplementary Materials: The following supporting information can be downloaded at <https://www.mdpi.com/article/10.3390/agriculture14030464/s1>, Text S1: Determination of basic physico-chemical properties and heavy metal concentration in tested soil; Table S1: Chemical composition of PG, RM, PR, and L-PR; Table S2: Basic physical and chemical parameters of tested soil; Table S3: Basic physical and chemical properties of PG, RM, PR, and L-PR; Table S4: Procedure for the extraction of availability and fractions of As and Cd in soil; Figure S1: EDS images of PG, RM, PR, and L-PR.; Figure S2: O 1s and C 1s spectra on PR surface; Figure S3: Cd 3d spectra on L-PR surface; Figure S4: As 3d spectra on L-PR surface. Reference [69] is cited in the Supplementary Materials.

Author Contributions: Conceptualization, C.S. and Y.S.; methodology, C.S.; software, C.S., Z.G. and L.H.; validation, C.S., D.C. and Q.Z.; formal analysis, Y.S.; data curation, C.S.; writing—original draft preparation, C.S.; writing—review and editing, Y.S., M.T., L.H., Z.G. and T.C.; visualization, C.S.; supervision, Y.S.; project administration, C.S.; funding acquisition, C.S. All authors have read and agreed to the published version of the manuscript.

Funding: This research was funded by National Natural Science Foundation of China, grant number 41761071, Guizhou Provincial Science and Technology Projects, grant number QKHZC[2023]YB217, and the special fund for Science and Technology Innovation Teams of Shanxi Province, grant number 202304051001016.

Institutional Review Board Statement: Not applicable.

Data Availability Statement: Data are contained within the article.

Conflicts of Interest: Zhixi Geng is employed by the company “Beijing Zhongnong Jiayuan Eco-Engineering Technology Co., Ltd.”. The remaining authors declare that the research was conducted in the absence of any commercial or financial relationships that could be construed as a potential conflict of interest.

References

- Kim, H.S.; Kim, Y.J.; Seo, Y.R. An Overview of Carcinogenic Heavy Metal: Molecular Toxicity Mechanism and Prevention. *J. Cancer Prev.* **2015**, *20*, 232–240. [[CrossRef](#)]
- Deng, H.; Tu, Y.; Wang, H.; Wang, Z.; Li, Y.; Chai, L.; Zhang, W.; Lin, Z. Environmental behavior, human health effect, and pollution control of heavy metal(loid)s toward full life cycle processes. *Eco-Environ. Health* **2022**, *1*, 229–243. [[CrossRef](#)] [[PubMed](#)]
- Liu, H.-L.; Zhou, J.; Li, M.; Hu, Y.-m.; Liu, X.; Zhou, J. Study of the bioavailability of heavy metals from atmospheric deposition on the soil-pakchoi (*Brassica chinensis* L.) system. *J. Hazard. Mater.* **2019**, *362*, 9–16. [[CrossRef](#)] [[PubMed](#)]
- Chen, H.; Yang, X.; Wang, P.; Wang, Z.; Li, M.; Zhao, F.-J. Dietary cadmium intake from rice and vegetables and potential health risk: A case study in Xiangtan, southern China. *Sci. Total Environ.* **2018**, *639*, 271–277. [[CrossRef](#)] [[PubMed](#)]
- Nguyen, H.D.; Kim, M.-S. Interactions between cadmium, lead, mercury, and arsenic and depression: A molecular mechanism involved. *J. Affect. Disord.* **2023**, *327*, 315–329. [[CrossRef](#)] [[PubMed](#)]
- Huang, M.X.; Guan, Y.F.; Su, Z.X.; Tao, L. Interfacial Reactions between As(V) and Cd(II) Co-adsorption onto Various Mineral Surfaces. *Acta Pedol. Sin.* **2022**, *59*, 1583–1593.
- Duan, G.; Shao, G.; Tang, Z.; Chen, H.; Wang, B.; Tang, Z.; Yang, Y.; Liu, Y.; Zhao, F.-J. Genotypic and Environmental Variations in Grain Cadmium and Arsenic Concentrations Among a Panel of High Yielding Rice Cultivars. *Rice* **2017**, *10*, 9. [[CrossRef](#)]
- Yuan, Z.H.; Li, Q.H.; Ma, X.Y.; Han, M.S. Assessment of heavy metals contamination and water quality characterization in the Nanming River, Guizhou Province. *Environ. Geochem. Health* **2021**, *43*, 1273–1286. [[CrossRef](#)] [[PubMed](#)]
- Zhang, P.L.; Yao, J.F.; Liu, Y.L.; Zhang, W.Y.; Yin, X.F.; Tie, B.Q. Effect of Combined Application of an Enterobacter and Sulfur Fertilizer on Cadmium and Arsenic Accumulation in Rice. *Environ. Sci.* **2023**, *44*, 7036–7044. [[CrossRef](#)]
- Chen, N.C.; Zheng, Y.J.; He, X.F.; Li, X.F.; Zhang, X.X. Analysis of the Report on the national general survey of soil contamination. *J. Agro-Environ. Sci.* **2017**, *36*, 1689–1692.
- Chen, Z.L.; Qiu, R.L.; Zhang, J.S. Removed Technology of Heavy Metal Pollution in Soil. *Environ. Prot.* **2002**, *6*, 21–23.
- Zeng, X.B.; Li, L.F.; Mei, X.R. Heavy Metal Content in Soils of Vegetable-growing Lands in China and Source Analysis. *Sci. Agric. Sin.* **2007**, *40*, 2507–2517.
- Chen, H.X.; Xu, F.N.; Chen, Z.Z.; Jiang, O.Y.; Gustave, W.; Tang, X.J. Arsenic and cadmium removal from water by a calcium-modified and starch-stabilized ferromanganese binary oxide. *J. Environ. Sci.* **2020**, *96*, 186–193. [[CrossRef](#)]
- Xu, X.; Luo, P.; Li, S.; Zhang, Q.; Sun, D. Distributions of Heavy Metals in Rice and Corn and Their Health Risk Assessment in Guizhou Province. *Bull. Environ. Contam. Toxicol.* **2022**, *108*, 926–935. [[CrossRef](#)]
- Xiong, Y.; Yang, Y.Q.; Li, M.Z.; Lu, S.J. Study on Comprehensive Utilization of Phosphogypsum. *Res. Econ. Environ. Prot.* **2018**, *202*, 33–34+37. [[CrossRef](#)]
- Zhou, B.; Zhu, H.; Xu, S.; Du, G.; Shi, S.; Liu, M.; Xing, F.; Ren, J. Effect of phosphogypsum on the properties of magnesium phosphate cement paste with low magnesium-to-phosphate ratio. *Sci. Total Environ.* **2021**, *798*, 149262. [[CrossRef](#)]
- Jovičević-Klug, M.; Souza Filho, I.R.; Springer, H.; Adam, C.; Raabe, D. Green steel from red mud through climate-neutral hydrogen plasma reduction. *Nature* **2024**, *625*, 703–709. [[CrossRef](#)] [[PubMed](#)]
- Zhen, L.; Chen, H.; Wang, H.; Qi, Y.; Gao, L.; Zhang, S. Comprehensive utilization status and development suggestions of phosphogypsum in China. *Phosphate Compd. Fertil.* **2017**, *32*, 33–35.
- Liu, W.; Chen, X.; Li, W.; Yu, Y.; Yan, K. Environmental assessment, management and utilization of red mud in China. *J. Clean. Prod.* **2014**, *84*, 606–610. [[CrossRef](#)]
- Liu, G.; He, M.; Chen, H.; Rashad, A.M.; Liang, Y. Study on the curing conditions on the physico-mechanical and environmental performance of phosphogypsum-based artificial aggregates. *Constr. Build. Mater.* **2024**, *415*, 135030. [[CrossRef](#)]
- Xie, L.Q.; Zhang, T.A.; Lv, G.Z.; Yang, J.L.; Wang, Y.X. The effect of NaOH on the direct calcification–carbonation method for processing of Bayer process red mud. *Green Process. Synth.* **2017**, *7*, 546–551. [[CrossRef](#)]
- Kushwaha, S.S.; Kishan, D.; Chauhan, M.S.; Khetawath, S. Stabilization of Red mud using eko soil enzyme for highway embankment. *Mater. Today Proc.* **2018**, *5*, 20500–20512. [[CrossRef](#)]
- Yang, Y.H.; Shu, D.T.; Ning, P. Kinetics and thermodynamics of adsorption of Cu^{2+} , Zn^{2+} , Pb^{2+} and Cd^{2+} by modified phosphogypsum induced by microwave field. *J. Cen. South Univ.* **2013**, *44*, 2157–2164.
- Zhang, L.Z.; Zhang, Y.X.; Zhang, X.F.; Tan, X.M.; Lv, Z.H. Research Progress of Resource Utilization of Phosphogypsum in China. *Conserv. Util. Min. Res.* **2019**, *39*, 14–18+92. [[CrossRef](#)]
- Wang, Y. Preparation and Properties of Lanthanum-Modified Adsorbents for Phosphorus Removal. Master's Thesis, Beijing University of Chemical Technology, Beijing, China, 2021.
- Li, J.; Zu, Y.Q.; Li, G.; Sun, G.X. Mechanism of As(V) Removal from Water by Lanthanum and Cerium Modified Biochars. *Environ. Sci.* **2018**, *39*, 2211–2218. [[CrossRef](#)]
- Chen, Y.; Xu, R.; Li, Y.; Liu, Y.; Wu, Y.; Chen, Y.; Zhang, J.; Chen, S.; Yin, H.; Zeng, Z.; et al. La(OH)₃-modified magnetic CoFe₂O₄ nanocomposites: A novel adsorbent with highly efficient activity and reusability for phosphate removal. *Colloids Surf. A Physicochem. Eng. Asp.* **2020**, *599*, 124870. [[CrossRef](#)]
- GB 15618-2018; Soil Environmental Quality Risk Control Standard for Soil Contamination of Agricultural Land. Ministry of Ecology and Environment the People's Republic of China: Beijing, China, 2018.
- Mohammad, A.S.G. Study of the Adsorption Efficiency of an Eco-Friendly Carbohydrate Polymer for Contaminated Aqueous Solution by Organophosphorus Pesticide. *Open J. Org. Polym. Mater.* **2014**, *4*, 16–28.

30. Huang, X.; Zhao, H.; Hu, X.; Liu, F.; Ji, P. Optimization of Preparation Technology for Modified Coal Fly Ash and Its Adsorption Properties for Cd²⁺. *J. Hazard. Mater.* **2020**, *392*, 122461. [[CrossRef](#)]
31. Inyang, M.; Gao, B.; Yao, Y.; Xue, Y.; Zimmerman, A.R.; Pullammanappallil, P.; Cao, X. Removal of heavy metals from aqueous solution by biochars derived from anaerobically digested biomass. *Bioresour. Technol.* **2012**, *110*, 50–56. [[CrossRef](#)]
32. Zhang, H.; Yue, X.; Li, F.; Xiao, R.; Zhang, Y.; Gu, D. Preparation of rice straw-derived biochar for efficient cadmium removal by modification of oxygen-containing functional groups. *Sci. Total Environ.* **2018**, *631*, 795–802. [[CrossRef](#)]
33. Sahuquillo, A.; Rigol, A.; Rauret, G. Overview of the use of leaching/extraction tests for risk assessment of trace metals in contaminated soils and sediments. *Trends Anal. Chem.* **2003**, *22*, 152–159. [[CrossRef](#)]
34. Wenzel, W.W.; Kirchbaumer, N.; Prohaska, T.; Stingeder, G.; Adriano, D.C. Arsenic fractionation in soils using an improved sequential extraction procedure. *Anal. Chim. Acta* **2001**, *436*, 309–323. [[CrossRef](#)]
35. Fathollahzadeh, H.; Kaczala, F.; Bhatnagar, A.; Hogland, W. Speciation of metals in contaminated sediments from Oskarshamn Harbor, Oskarshamn, Sweden. *Environ. Sci. Pollut. Res.* **2014**, *21*, 2455–2464. [[CrossRef](#)] [[PubMed](#)]
36. Ennaciri, Y.; Alaoui-Belghiti, H.E.; Bettach, M. Comparative study of K₂SO₄ production by wet conversion from phosphogypsum and synthetic gypsum. *J. Mater. Res. Technol.* **2019**, *8*, 2586–2596. [[CrossRef](#)]
37. Yan, W.; Zeng, B.L.; Meng, J.; Wang, S.M.; Liang, S.W. Study on the Identification of Gypsum Fibrosum with FTIR. *Spectrosc. Spectr. Anal.* **2016**, *36*, 2098–2103.
38. Li, C. Preparation and Application Study of Heavy Metal Adsorbents Based on Red Mud. Master's Thesis, Guizhou University, Guiyang, China, 2021.
39. Cao, J.L.; Yan, Z.L.; Deng, Q.F.; Yuan, Z.Y.; Zhang, Z.Y. Homogeneous precipitation method preparation of modified red mud supported Ni mesoporous catalysts for ammonia decomposition. *Catal. Sci. Technol.* **2014**, *4*, 361–368. [[CrossRef](#)]
40. Cao, J.L.; Yan, Z.L.; Deng, Q.F.; Yan, W.; Yong, Y.Z. Mesoporous modified-red-mud supported Ni catalysts for ammonia decomposition to hydrogen. *Int. J. Hydrog. Energy* **2014**, *39*, 5747–5755. [[CrossRef](#)]
41. Li, Z.; Zhang, J.; Li, S.; Lin, C.; Liu, C. Feasibility of preparing red mud-based cementitious materials: Synergistic utilization of industrial solid waste, waste heat, and tail gas. *J. Clean. Prod.* **2020**, *285*, 124896. [[CrossRef](#)]
42. Chen, M.X. Preparation of Lanthanum Modified Zeolite and Passivation Effect on Phosphorus in the Sediments of the River. Master's Thesis, Guangzhou University, Guiyang, China, 2022.
43. He, Y.P.; Yang, S.J. Application of BET Specific Surface Area Method in Materials Research. *Adv. Fine Petrochem* **2018**, *19*, 52–56. [[CrossRef](#)]
44. Kam, S.K.; Kang, K.H.; Lee, M.G. Adsorption Characteristics of Acetone, Benzene and Methyl Mercaptan according to the Surface Chemistry and Pore Structure of Activated Carbons Prepared from Waste Citrus Peel in the Fixed Bed Adsorption Reactor. *Appl. Chem. Eng.* **2018**, *29*, 237–243.
45. Anuar, S.A.; Isahak, W.N.R.W.; Masdar, M.S. Carbon nanoflake hybrid for biohydrogen CO₂ capture: Breakthrough adsorption test. *Int. J. Energy Res.* **2020**, *44*, 3148–3159. [[CrossRef](#)]
46. Wu, J.; Wang, T.; Wang, J.; Zhang, Y.; Pan, W.P. A novel modified method for the efficient removal of Pb and Cd from wastewater by biochar: Enhanced the ion exchange and precipitation capacity. *Sci. Total Environ.* **2020**, *754*, 142150. [[CrossRef](#)]
47. Li, H.; Lin, H.; Liang, Y.; Feng, M.; Zhou, Z.; Liang, Z.; Lu, Y.; Zeng, H.; Chen, G. Simultaneous removal of cadmium(II) and arsenic(III) from aqueous solutions using pyrite-modified biochar: Effects and mechanisms. *Chem. Eng. Res. Des.* **2023**, *200*, 344–355. [[CrossRef](#)]
48. Lin, S.; Yang, X.; Liu, L.; Li, A.; Qiu, G. Electrosorption of cadmium and arsenic from wastewaters using nitrogen-doped biochar: Mechanism and application. *J. Environ. Manag.* **2022**, *301*, 113921. [[CrossRef](#)] [[PubMed](#)]
49. Qiao, Q.; Yang, X.; Liu, L.; Luo, Y.; Tan, W.; Liu, C.; Dang, Z.; Qiu, G. Electrochemical adsorption of cadmium and arsenic by natural Fe-Mn nodules. *J. Hazard. Mater.* **2020**, *390*, 122165. [[CrossRef](#)] [[PubMed](#)]
50. Lin, L.; Song, Z.; Khan, Z.H.; Liu, X.; Qiu, W. Enhanced As(III) removal from aqueous solution by Fe-Mn-La-impregnated biochar composites. *Sci. Total Environ.* **2019**, *686*, 1185–1193. [[CrossRef](#)]
51. Zhang, W.; Fu, J.; Zhang, G.X. Enhanced arsenate removal by novel Fe-La composite (hydr)oxides synthesized via coprecipitation. *Chem. Eng. J.* **2014**, *251*, 69–79. [[CrossRef](#)]
52. Wang, Y.Y.; Ji, H.Y.; Lu, H.H.; Liu, Y.X.; Yang, R.Q.; He, L.L.; Yang, S.M. Simultaneous removal of Sb(III) and Cd(II) in water by adsorption onto a MnFe₂O₄-biochar nanocomposite. *RSC Adv.* **2018**, *8*, 3264–3273. [[CrossRef](#)]
53. Ding, H.L.; Zhang, X.N.; Yang, H.; Luo, X.G.; Lin, X.Y. Highly efficient extraction of thorium from aqueous solution by fungal mycelium-based microspheres fabricated via immobilization. *Chem. Eng. J.* **2019**, *368*, 37–50. [[CrossRef](#)]
54. Cai, T.; Du, H.; Liu, X.; Tie, B.; Zeng, Z. Insights into the removal of Cd and Pb from aqueous solutions by NaOH-EtOH-modified biochar. *Environ. Technol. Innov.* **2021**, *24*, 102031. [[CrossRef](#)]
55. Bogusz, A.; Oleszczuk, P.; Dobrowolski, R. Application of laboratory prepared and commercially available biochars to adsorption of cadmium, copper and zinc ions from water. *Bioresour. Technol.* **2015**, *196*, 540–549. [[CrossRef](#)] [[PubMed](#)]
56. Jin, H.; Hanif, M.U.; Capareda, S.; Chang, Z.; Ai, Y. Copper(II) removal potential from aqueous solution by pyrolysis biochar derived from anaerobically digested algae-dairy-manure and effect of KOH activation. *J. Environ. Chem. Eng.* **2015**, *4*, 365–372. [[CrossRef](#)]
57. Li, H.; Dong, X.; Da Silva, E.B.; De Oliveira, L.M.; Chen, Y.; Ma, L.Q. Mechanisms of metal sorption by biochars: Biochar characteristics and modifications. *Chemosphere* **2017**, *178*, 466–478. [[CrossRef](#)]

58. Su, Z.X.; Liu, S.H.; Guan, Y.F.; Tao, L. Cadmium and Arsenic Interactions During Co-sorption onto Goethite. *Environ. Sci.* **2023**, *44*, 3970–3977. [[CrossRef](#)]
59. Liu, J.; Zhu, R.; Liang, X.; Ma, L.; Molinari, M. Synergistic adsorption of Cd(II) with sulfate/phosphate on ferrihydrite: An in situ ATR-FTIR/2D-COS study. *Chem. Geol.* **2018**, *477*, 12–21. [[CrossRef](#)]
60. Wu, J.Z.; Huang, D.; Liu, X.M.; Meng, J.; Tang, C.X.; Xu, J.M. Remediation of As(III) and Cd(II) co-contamination and its mechanism in aqueous systems by a novel calcium-based magnetic biochar. *J. Hazard. Mater.* **2018**, *348*, 10–19. [[CrossRef](#)]
61. Pérez-Esteban, J.; Escolástico, C.; Masaguer, A.; Vargas, C.; Moliner, A. Soluble organic carbon and pH of organic amendments affect metal mobility and chemical speciation in mine soils. *Chem Environ. Toxicol. Risk Assess.* **2014**, *103*, 164–171. [[CrossRef](#)]
62. Li, Z.; Wang, L.; Wu, J.; Xu, Y.; Wang, F.; Tang, X.; Xu, J.; Ok, Y.S.; Meng, J.; Liu, X. Zeolite-supported nanoscale zero-valent iron for immobilization of cadmium, lead, and arsenic in farmland soils: Encapsulation mechanisms and indigenous microbial responses. *Environ. Pollut.* **2020**, *260*, 114098. [[CrossRef](#)]
63. Wu, J.; Li, Z.; Huang, D.; Liu, X.; Xu, J. A novel calcium-based magnetic biochar is effective in stabilization of arsenic and cadmium co-contamination in aerobic soils. *J. Hazard. Mater.* **2020**, *387*, 122010. [[CrossRef](#)]
64. Wang, X.; Yu, H.Y.; Li, F.; Liu, T.; Wu, W.; Liu, C.; Liu, C.; Zhang, X. Enhanced immobilization of arsenic and cadmium in a paddy soil by combined applications of woody peat and Fe(NO₃)₃: Possible mechanisms and environmental implications. *Sci. Total Environ.* **2019**, *649*, 535–543. [[CrossRef](#)]
65. Li, Q.; Zhang, P.; Zhou, H.; Peng, P.Q.; Zhang, K.; Mei, J.X.; Li, J.; Liao, B.H. Effects of Cd-resistant bacteria and calcium carbonate plus sepiolite on Cd availability in contaminated paddy soil and on Cd accumulation in brown rice grains. *Ecotoxicol. Environ. Saf.* **2020**, *195*, 110492. [[CrossRef](#)] [[PubMed](#)]
66. Ainiwaer, M.; Zhang, T.; Zhang, N.; Yin, X.X.; Su, S.M.; Wang, Y.A.; Zhang, Y.; Zeng, X.B. Synergistic removal of As(III) and Cd(II) by sepiolite-modified nanoscale zero-valent iron and a related mechanistic study. *J. Environ. Manag.* **2022**, *319*, 115658. [[CrossRef](#)] [[PubMed](#)]
67. Sun, Y.; Xu, Y.; Xu, Y.; Wang, L.; Liang, X.; Li, Y. Reliability and stability of immobilization remediation of Cd polluted soils using sepiolite under pot and field trials. *Environ. Pollut.* **2016**, *208*, 739–746. [[CrossRef](#)] [[PubMed](#)]
68. Cui, J.; Jin, Q.; Li, Y.; Li, F. Oxidation and removal of As(III) from soil using novel magnetic nanocomposite derived from biomass waste. *Environ. Sci.-Nano* **2019**, *6*, 478–488. [[CrossRef](#)]
69. Lu, R. *Methods of Soil Agricultural Chemical Analysis*; China Agricultural Science and Technology Press: Beijing, China, 2000.

Disclaimer/Publisher's Note: The statements, opinions and data contained in all publications are solely those of the individual author(s) and contributor(s) and not of MDPI and/or the editor(s). MDPI and/or the editor(s) disclaim responsibility for any injury to people or property resulting from any ideas, methods, instructions or products referred to in the content.